The slip distributions of the 1952 and 2025 Kamchatka earthquakes from tsunami waveforms recorded around the Pacific Ocean

Yushiro Fujii

International Institute of Seismology and Earthquake Engineering

Building Research Institute, Tsukuba, Japan

fujii@kenken.go.jp

https://orcid.org/0000-0001-7686-1841

Kenji Satake (corresponding author)

Department of Earth Sciences, National Central University, Taoyuan, Taiwan

satake@nct.edu.tw

https://orcid.org/0000-0002-3368-3085

Key points

1. The 2025 Kamchatka earthquake has the largest slip (~ 9m) at 200 – 400 km SW of the epicenter at a shallow plate interface
2. The tsunami heights and waveforms of the 2025 and 1952 earthquakes were very similar
3. The 1952 Kamchatka earthquake had an overall size and slip distribution similar to the 2025 event, although the interval was only 73 years

Abstract

The July 2025 Kamchatka earthquake (Mw 8.8) generated Pacific-wide tsunamis. Inversion of 40 DART bottom pressure records around the Pacific Ocean revealed a large (~ 9 m) slip at 200 – 400 km southwest of the epicenter, closely matching the USGS finite fault model based on teleseismic data. In this region, a similarly large megathrust earthquake (M ~ 9) occurred in 1952. The tsunami waveforms recorded at tide gauge stations around the Pacific Ocean were very similar to those of the 2025 earthquake. We also made an inversion of the 1952 tide gauge data to estimate the slip distribution and clock correction at each station, considering the elasticity of the Earth and sea water and the station corrections. The 1952 slip distribution is similar to that of 2025, except for the depth of the largest slip and the northern slip where foreshock and aftershocks occurred in 2025.

Plain Language Summary

The July 2025 Kamchatka earthquake (Mw 8.8) was the seventh-largest earthquake in the last century. This earthquake was somewhat unexpected, occurring only 73 years after a similar giant earthquake at the same location in 1952. Typically, such giant megathrust earthquakes recur at intervals of a few to several centuries. This study estimated the sizes and slip distributions of both the 1952 and 2025 earthquakes using state-of-the-art tsunami simulation methods while accounting for potential clock errors of the paper analog records of the 1952 tsunami. The overall sizes and the slip distributions of both earthquakes were generally similar, except for the depth of the largest slip and the 1952 slip north of the epicenter. Since the largest slip exceeded cumulative slip due to the plate motion, the locations of the largest slip may have been slightly different for the 1952 and 2025 earthquakes.

1. Introduction

A great earthquake (M 8.8) occurred off Kamchatka peninsula on 2025 July 29 at 23:24:52.5 (UTC), or in the morning of July 30 in local time. According to USGS (United States Geological Survey), the epicenter is 52.4948°N 160.2395°E and the depth is 35 km. The USGS also provided several versions of finite-source models (slip distribution on the fault) (https://earthquake.usgs.gov/earthquakes/eventpage/us6000qw60/finite-fault), that shows the large slip occurred 100 – 400 km southwest of the epicenter, while a large foreshock (M 7.4 on July 20) and aftershocks (M 7.4 on Sep. 13 and M 7.8 on Sep. 18) occurred near or north of the epicenter.

The occurrence of this earthquake is somewhat surprising because a great earthquake with a similar size (M 9.0) occurred in 1952 at a similar location. According to USGS, the origin time was November 4 16:58:30 (UTC) and the hypocenter was 52.623°N, 159.779°E, 22 km. The moment magnitude was estimated from the free oscillation of the Earth (Kanamori, 1976). The 1952 earthquake generated a Pacific-wide tsunami. Johnson and Satake (1999) conducted a tsunami waveform inversion and estimated the slip distribution of the 1952 event. The largest slip was located at a deep part of the subducting plate interface. Based on near-field tsunami data, MacInnes et al. (2010) concluded that the high slip region might have been shallower.

The analysis of Johnson and Satake (1999) had some limitations from a modern perspective. First, the effects of elastic Earth and sea water for long-distance traveling tsunami (Watada et al., 2014), which is known to produce ~1% delay compared to linear long wave, were not considered. Second, the tsunami simulation grids were relatively coarse (5 min and 1 min of the arc), limiting the accuracy of tsunami travel time and waveforms at tide gauge stations. Third, possible clock errors of the analog tide gauge records in the 1950s were not considered.

In this paper, we estimate the slip distributions of both the 2025 and 1952 earthquakes from tsunami waveforms, by considering the above limitations of the previous study. We first estimate the 2025 source using the DART (Deep-ocean Assessment and Reporting of Tsunamis) data, considering the elastic effects of the Earth and sea water. We then simulate the tsunami at tide gauge stations where both 1952 and 2025 tsunamis were recorded, and measure the time difference between the observed and simulated waveforms, i.e., estimate the station corrections. We further conduct inversions of the 1952 tide gauge records, to estimate the slip distribution and clock error at each station, by considering the elastic effects and the station corrections.

2. Data

The 2025 tsunami was recorded on DART bottom pressure gauges and coastal tide gauges. We used tsunami waveforms recorded at 40 DART stations (Figure 1), downloaded from NOAA National Data Buoy Center (https://www.ndbc.noaa.gov/obs.shtml). Nearly half of them were recorded in the western Pacific Ocean, and the other half were in the eastern Pacific Ocean, providing good azimuthal coverage. In addition, we selected 37 tide gauge stations that recorded both the 2025 and 1952 tsunamis. Among them, 10 were in Japan, 8 in the Pacific Ocean, 12 in North America, and 7 in South America (Figure 1). The tide gauge data were downloaded from UNESCO IOC sea level station monitoring facility (https://www.ioc-sealevelmonitoring.org/). Several tide gauge records in Japan were digitized from the Japan Meteorological Agency's press release (JMA, 2025). The tsunami waveforms are shown in Figure 2.

The 1952 tsunami was recorded on coastal tide gauges (with possible clock errors). We digitized the analog records from United States Coast and Geodetic Survey (USCGS, 1953), NOAA/NCEI, and Central Meteorological Organization (CMO, 1953) for the Japanese records. They are also shown in Figure 2.

The sampling intervals of digital and digitized tsunami waveforms are all 1 min.

3. Method: Tsunami Waveform Inversion

To estimate the slip distribution on an earthquake fault, we placed 24 subfaults as shown in Figure 3 and Table 1. The subfault size is 100 km x 50 km. The strike is fixed at 218° and the slip angle at 90°. The top depth and the dip angles vary from 0 km to 47 km and from 10° to 30° along with Slab 2.0 model (Hayes et al., 2018). We consider the rupture propagation with a constant rupture velocity of 2.5 km/s; the starting time of slip on each subfault is calculated from the epicentral distance divided by the rupture velocity. The rise time of slip on each subfault is fixed at 30 sec. The seafloor displacement due to a unit amount of slip (1 m) is computed by the formulas of Okada (1985) with the effects of horizontal displacement and seafloor slope (Tanioka and Satake, 1996).

The tsunami Green's functions are computed based on the linear long wave theory (Fujii and Satake, 2024) in the region shown in Figure 1 (120°E–68°W and 55° S–61°N). The phase corrections for the elasticity of the Earth, compressibility of sea water, and gravitational potential variation (Watada et al., 2014) have been applied to the Green's functions. We employed the phase difference table developed by Ho et al. (2017), which further takes into account the effects of stratified ocean layers. The 15 arc-sec bathymetry grid data from GEBCO 2024 (GEBCO Compilation Group, 2024) were resampled with a 24 arc-sec grid interval.

We first made a tsunami waveform inversion of the 2025 DART data. Because their locations are in the deep ocean, free from nonlinear and coastal topographical effects, and have the good azimuthal coverage, we believe that the DART inversion provides the most reliable results.

We then computed the tsunami waveforms from the DART inversion, and compared them with the observations, to measure the timing shift at each station. These shifts are due to our numerical simulation with a rather coarse (24” or ~740 m) grid size, hence we considered them as station corrections of our numerical simulation (Table S1). We also made an inversion of the 2025 tsunami waveforms at tide gauge stations after applying the station corrections.

For the 1952 tsunami data, the possible clock errors are included. Therefore, we simultaneously estimate the slip distribution and the clock error at each station by the OTA (Optimal Time Alignment) method (Romano et al., 2016; Ho et al., 2019).

4. Results

The slip distributions from the 2025 DART and tide gauge (TG) inversions are shown in Figure 3a and 3b, respectively, as well as in Table 1. The DART inversion shows large (> 9 m) slip in three subfaults at distances of 200–400 km SW of the epicenter with depth of 0 – 26 km (below seafloor). The average slip is 3.1 m, providing a total seismic moment of 1.87×10^{22} Nm (Mw 8.8), assuming the rigidity of 50 GPa. Comparison of the observed and simulated tsunami waveforms at DART stations (Figure 4) shows that they agree very well at all the stations. Slight discrepancies in the tailing waves at nearby stations (21416, 21415, 21414, 46413) are due to dispersion effects, which are not included in our simulation. Figure 4 also shows simulated waveforms without considering the elastic effects. At far-field stations (travel times > 420 min or 7 hours), the simulated waveforms arrive clearly earlier, because the elastic effects cause about 1 % slower phase velocity.

The 2025 TG inversion yields a similar result, but slightly larger average slip (3.8 m) and seismic moment (2.28×10^{22} Nm or Mw 8.8). The large slips occur at similar subfaults, but the amounts are larger (> 10 m). Figures S1 and S2 show the comparison of the observed and simulated tsunami waveforms at the DART and tide gauge stations. The simulated waveforms are very similar to the observed, including at Kahului where the largest tsunami amplitude was recorded (not used for the inversion).

The 1952 slip distribution also has a large slip on subfaults at 200–400 km SW of the epicenter and the shallowest region (Figure 3c). The average slip (5 m) and the largest slip (18 m) are larger than those of the 2025 models (both DART and TG inversions). The seismic moment of 2.98×10^{22} Nm (Mw 8.9) is also larger than the 2025 earthquake. Two notable differences between the 2025 and 1952 slip distributions are the depth of the largest slip and the large slip north of the epicenter. The largest slip of the 2025 earthquake appeared at subfaults 4B and 5B (the depth of 9 – 20 km beneath seafloor), while the largest slip of the 1952 earthquake appeared at the shallowest subfaults (4A and 5A, depth 0 – 9 km). The northern slip (subfault 1D) appears only in 1952; this northern slip is required to explain the large and longer duration of the tige stations in the Aleutian Islands (Adak and Dutch Harbor). The 2025 earthquake was preceded by a foreshock (M 7.4) and followed by aftershocks (M 7.4, M 7.8) to the north of the epicenter. No such large (M ≥ 7) earthquake occurred before or after the 1952 earthquake in the source region. The lack of the northern slip may be due to the foreshock and aftershocks in 2025.

5. Discussion

The slip distribution of the 1952 Kamchatka earthquake, a large slip in the southwestern and shallow part of the source region, is quite different from that of Johnson and Satake (1999). The main reason is their lack of consideration of the elastic effects of the Earth and sea water, that were found by Watada et al. (2014). To confirm this, we made an inversion of the 1952 tsunami waveforms without making phase shifts for the Green's functions. The result (Figure 3d) shows large slips in the deeper part of the subduction zone, somewhat similar to that of Johonson and Satake (1999).

In the source region of the 2025 and 1952 earthquakes, giant earthquakes also occurred in 1841 and 1737. Unlike the 1952 and 2025 earthquakes, the 1841 and 1737 earthquakes did not leave tsunami waveforms on tide gauges, but the tsunami runup heights were recorded (NOAA/NCEI, Table S2). The tsunami heights in Hawaii were mostly 1 – 2 m, although the maximum of 4.6 m (1841) and 3.7 m (1952) were recorded. In general, the tsunami heights of these events were similar, and the tsunami magnitude (Mt) was about 9 (Abe, 1979). Gusev and Shumilina (2004) concluded that these earthquakes were of giant (M~9) size, and estimated their recurrence intervals as 85 – 100 years (10 – 11.8 events in 1,000 years). Based on tsunami deposits, Pinegina et al. (2018, 2020) estimated that the recurrence of "typical" earthquakes as ~130 years (30 events / 4,000 years). They also estimated the recurrence of "full-length" events, with coastal subsidence, as ~1,300 years (3 events / 4,000 years). These intervals of giant (M~9) earthquakes are shorter than those of other subduction zones (Satake and Atwater, 2007), and the 73 years between the 1952 and 2025 events may not be unusually short.

The convergence rate of the subducting Pacific Plate and the overlying North American plate is ~ 8 cm/year, and the estimated backslip rate from the GPS analysis is up to nearly 8 cm/year, indicating a full coupling of the plate interface (Burgman et al., 2005). The interval between the last (1952) and the present (2025) earthquakes is only 73 years. If the strain was completely released in 1952, the accumulated slip would be 5.8 m, while the largest slip in the 2025 event was ~ 9 m. As we have seen in the previous section, the largest slip appeared at different subfaults between the 1952 and 2025 events, despite that the overall patterns are similar. The largest slip occurred at the shallowest subfault in 1952, but slightly deeper subfaults in 2025. Such a difference in slip depth also occurred along the Japan Trench (Satake et al., 2017). In 1896, the Meiji Sanriku tsunami earthquake ruptured with a large slip of ~ 20 m at a depth of 3.5 – 7 km, where the slip of the 2011 Tohoku earthquake was 3 – 14 m. The largest slip of the Tohoku earthquake (20 – 36 m) occurred at shallower depth (0 – 3.5 km beneath seafloor), thus the shallowest slips were complementary. A similar complementary slip might have occurred in the Kamchatka subduction zone. During the 1952 Kamchatka earthquake, the accumulated strain had not been fully released, hence the slip amount in the 2025 earthquake may have been greater than the 73-year slip deficit.

6. Conclusions

The slip distributions of the 2025 and 1952 Kamchatka earthquakes were estimated from the tsunami waveforms recorded around the Pacific Ocean. The largest and average slips were ~ 9 m and 3.1 m for the 2025 event, and ~ 18 m and 5 m for the 1952 event. The seismic moments were 1.9×10^{22} Nm (Mw 8.8) for the 2025 earthquake and 3.0×10^{22} Nm (Mw 8.9) for the 1952 earthquake. The large slip appeared at 200 – 400 km southwest of the epicenter for both events, but the depth is slightly different. The largest slip appeared at a shallower depth in 1952 than in the 2025 event. This difference, or complementary slip, can explain the shorter interval than expected from backslip rate (~ 8 m/century) estimated from GPS analysis (Burgman et al., 2005).

Conflict of Interest Disclosure

The authors declare there are no conflicts of interest for this manuscript.

Acknowledgments

Kenji Satake is supported by Yushan Fellowship from Ministry of Education, Taiwan government. All figures were generated using Generic Mapping Tools (Wessel and Smith,1998). We thank Ms. Yoshie Fujii for her support in digitizing the tide gauge records and converting the tsunami waveform data.

Open Research

The tsunami waveforms of the 2025 Kamchatka earthquake are available at the NOAA Nation Data Buoy Center (https://www.ndbc.noaa.gov/obs.shtml) and UNESCO IOC sea level station monitoring facility (https://www.ioc-sealevelmonitoring.org/). The 1952 tsunami waveforms are available from publications of United States Coast and Geodetic Survey (1953) and Central Meteorological Organization (1953), as well as at NCEI/WDS Global Historical Tsunami Database (https://www.ncei.noaa.gov/products/natural-hazards/tsunamis-earthquakes-volcanoes/tsunamis) doi:10.7289/V5PN93H7

References

Abe, K. (1979), Size of great earthquakes of 1837–1974 inferred from tsunami data, *J. Geophys. Res*., 84(B4), 1561–1568. doi:10.1029/JB084iB04p01561.

Bürgmann, R., Kogan, M.G., Steblov, G.M., Hilley, G., Levin, V.E., and Apel, E. (2005), Interseismic coupling and asperity distribution along the Kamchatka subduction zone, *J. Geophys. Res.*, 110, B07405. doi:10.1029/2005JB003648.

Gusev, A.A. and Shumilina, L.S. (2004), Recurrence of Kamchatka strong earthquakes on a scale of moment magnitudes, *Izvestiya, Physics of the Solid Earth*, 40(3), 206-215. https://ns.emsd.ru/~gusev/2004/gusev_2004_recurrece.pdf

Central Meteorological Observatory (1953), Report of the 1952 Kamchatka earthquake and tsunami (in Japanese), *Quarterly J. Seismology*, 18(1), 1-48. https://www.jma.go.jp/jma/kishou/books/kenshin/kenshin1.html

Fujii, Y. and Satake, K. (2024), Modeling the 2022 Tonga eruption tsunami recorded on ocean bottom pressure and tide gauges around the Pacific, *Pure Appl. Geophys.,* 181, 1793–1809. doi: 10.1007/s00024-024-03477-1

GEBCO Compilation Group (2024), GEBCO 2024 Grid. doi:10.5285/1c44ce99-0a0d-5f4f-e063-7086abc0ea0f

Hayes, G.P., Moore, G.L., Portner, D.E., Hearne, M., Flamme, H. Furtney, M., and Smoczyk, G.M. (2018), Slab2, a comprehensive subduction zone geometry model, *Science*, 362, 58-61. doi:10.1126/science.aat4723

Ho, T.-C., Satake, K., and Watada, S. (2017), Improved phase corrections for transoceanic tsunami data in spatial and temporal source estimation: application to the 2011 Tohoku earthquake, *J. Geophys. Res.,* 122, 10,155–10,175. doi:10.1002/2017JB015070

Ho, T.-C., Satake, K., Watada, S., and Fujii, Y. (2019), Source estimate for the 1960 Chile earthquake from joint inversion of geodetic and transoceanic tsunami data, *J. Geophys. Res.,* 124*,* 2812–2828. doi:10.1029/2018JB016996

Japan Meteorological Agency (2025), Regarding the Earthquake Near the Kamchatka Peninsula Around 08:25 on July 30, 2025 (Fourth Report) (in Japanese), https://www.jma.go.jp/jma/press/2507/31a/202507311115.html

Johnson, J.M. and Satake, K. (1999), Asperity distribution of the 1952 great Kamchatka earthquake and its relation to future earthquake potential in Kamchatka, *Pure Appl. Geophys*., 154, 541-553. doi:10.1007/s000240050243

Kanamori, H. (1976), Re-examination of the earth's free oscillations excited by the Kamchatka earthquake of November 4, 1952, *Physics Earth Planet. Inter*., 11(3), 216-226. doi: 10.1016/0031-9201(76)90066-2

MacInnes, B.T., Weiss, R., Bourgeois, J, and Pinegina, T.K. (2010), Slip distribution of the 1952 Kamchatka great earthquake based on near-field tsunami deposits and historical records, *Bull. Seism. Soc. Am*., 100 (4),1695–1709. doi:10.1785/0120090376

Okada, Y. (1985), Surface deformation due to shear and tensile faults in a half-space, *Bull. Seism. Soc. Am*., 75 (4), 1135–1154. doi: 10.1785/BSSA0750041135

Pinegina, T.K., Bazanova, L.I., Zelenin, E.A., Bourgeois, J., Kozhurin, A.I., Medvedev, I.P., and Vydrin, D.S. (2018), Holocene tsunamis in Avachinsky Bay, Kamchatka, Russia, *Pure Appl. Geophys*., 175, 1485–1506. doi:10.1007/s00024-018-1830-0.

Pinegina,T.K., Bourgeois, J.,vBazanova, L.I., Zelenin, E.A., Krasheninnikov, S.P., and Portnyagin, M.V. (2020), Coseismic coastal subsidence associated with unusually wide rupture of prehistoric earthquakes on the Kamchatka subduction zone: A record in buried erosional scarps and tsunami deposits, *Quaternary Science Reviews*, 233,106171. doi:10.1016/j.quascirev.2020.106171.

Romano, F., Piatanesi, A., Lorito, S., Tolomei, C., Atzori, S., and Murphy, S. (2016). Optimal time alignment of tide-gauge tsunami waveforms in nonlinear inversions: Application to the 2015 Illapel (Chile) earthquake, *Geophys. Res. Lett.*, 43, 11,226–11,235. doi:10.1002/2016GL071310

Satake, K. and Atwater, B.F. (2007), Long-term perspectives on giant earthquakes and tsunamis at subduction zones, *Annu. Rev. Earth Planet. Sci.*, 35, 349-374. doi:10.1146/annurev.earth.35.031306.140302

Satake, K., Fujii, Y., and Yamaki, S. (2017), Different depths of near-trench slips of the 1896 Sanriku and 2011 Tohoku earthquakes, *Geoscience Letters*, 4:33. doi:10.1186/s40562-017-0099-y

Tanioka, Y. and Satake, K. (1996), Tsunami generation by horizontal displacement of ocean bottom, *Geophys. Res. Lett.*, 23, 861-864. doi:10.1029/96GL00736

US Coast and Geodetic Survey (1953), The tsunami of November 4,1952 as recorded at tide gauge stations, U.S. Department of commerce, Special Publication No.300, 62pp.

Watada, S., Kusumoto, S., and Satake, K. (2014), Traveltime delay and initial phase reversal of distant tsunamis coupled with the self-gravitating elastic Earth, *J. Geophys. Res.*, 119 (5), 4287-4310. doi:10.1002/2013JB010841

Wessel, P., and Smith, W. H. (1998), New, improved version of generic mapping tools released, *EOS Trans. Amer. Geophys. U.*, 79 (47), 579. doi:10.1029/98EO00426

Figure captions

Figure 1. DART and tide gauge stations that recorded the 2025 and 1952 tsunamis. The green squares are DART stations that recorded the 2005 tsunami. The yellow triangles are the tide gauge stations that recorded both the 1952 and 2025 tsunamis. Data sources such as IOC, CMO, JMA, USCGS and NCEI are listed in Table S1.

Figure 2. Comparison of 2025 and 1952 waveforms. The black curves are the 2025 waveforms, and the green curves are the 1952 waveforms with clock corrections (Table S1) applied. The horizontal axis is time since the origin time of the earthquakes.

Figure 3. The slip distributions of the 2025 and 1952 Kamchatka earthquakes. (a) The 2025 slip from the inversion of DART. The focal mechanism solution of the 2025 mainshock is from the USGS W-phase Moment Tensor solution. The locations of the foreshock and aftershocks are also shown. Aftershocks (red circles) within one day and foreshocks (green circles) larger than M 5 by USGS are also shown. (b) The 2025 slip from the tide gauge (TG) inversion. Subfault numbers along strike and dip directions are shown. (c)

The 1952 slip from the TG inversion considering the corrections of elasticity effects of the Earth and sea water (Watada et al., 2014). The red star indicates the epicenter determined by USGS. (d) The 1952 slip obtained without considering the elasticity effects.

Figure 4. The 2025 tsunami waveforms at DART stations with synthetic waveforms from the DART inversion solution. The black curves are the observation, the red and blue curves are the synthetic waveforms with and without the corrections for the elasticity of the Earth and sea water (Watada et al., 2014; Ho et al., 2017). The gray horizontal bars show the time windows used for the inversion.

Table 1 Fault parameters and slips inverted from inversions

#	Lat. (deg)	Lon. (deg)	Depth (km)	Dip (deg)	Slip (m)		
					2025 DART	2025 TG	1952 TG
1A	52.70000	162.20000	0.0	10	0.52	0.00	0.00
2A	51.99133	161.28632	0.0	10	2.08	1.21	0.00
3A	51.28265	160.38717	0.0	10	5.91	7.59	7.02
4A	50.57397	159.50196	0.0	10	5.96	10.76	18.40
5A	49.86530	158.63013	0.0	10	9.37	9.95	17.47
6A	49.15662	157.77116	0.0	10	5.56	5.51	6.04
1B	52.97263	161.62415	8.68	20	0.00	0.00	0.00
2B	52.26396	160.71963	8.68	20	1.14	0.00	1.12
3B	51.55528	159.82926	8.68	20	7.85	5.99	4.16
4B	50.84661	158.95249	8.68	20	9.61	11.46	7.06
5B	50.13793	158.08877	8.68	20	9.15	12.60	7.25
6B	49.42926	157.23759	8.68	20	4.60	7.52	6.88
1C	53.23278	161.07124	25.78	25	0.42	3.05	3.39
2C	52.52410	160.17559	25.78	25	3.69	2.28	0.00
3C	51.81543	159.29373	25.78	25	3.09	3.77	8.04

4C	51.10675	158.42513	25.78	25	2.20	0.42	4.19
5C	50.39808	157.56926	25.78	25	3.62	1.49	7.64
6C	49.68940	156.72564	25.78	25	0.00	0.00	0.64
1D	53.48368	160.53473	46.91	30	0.00	0.00	14.01
2D	52.77500	159.64778	46.91	30	0.00	0.00	0.00
3D	52.06633	158.77425	46.91	30	0.00	1.26	0.00
4D	51.35765	157.91367	46.91	30	0.00	0.99	1.43
5D	50.64898	157.06547	46.91	30	0.00	5.17	4.56
6D	49.94030	156.22924	46.91	30	0.00	0.00	0.00
#: Subfault number. Lat., Lon., and Depth: Location and the top depth of the eastmost corners. Rigidity of 50 GP is assumed.				Mo (Nm)	1.87×10^{22}	2.28×10^{22}	2.98×10^{22}
				Mw	8.8	8.8	8.9

Figures

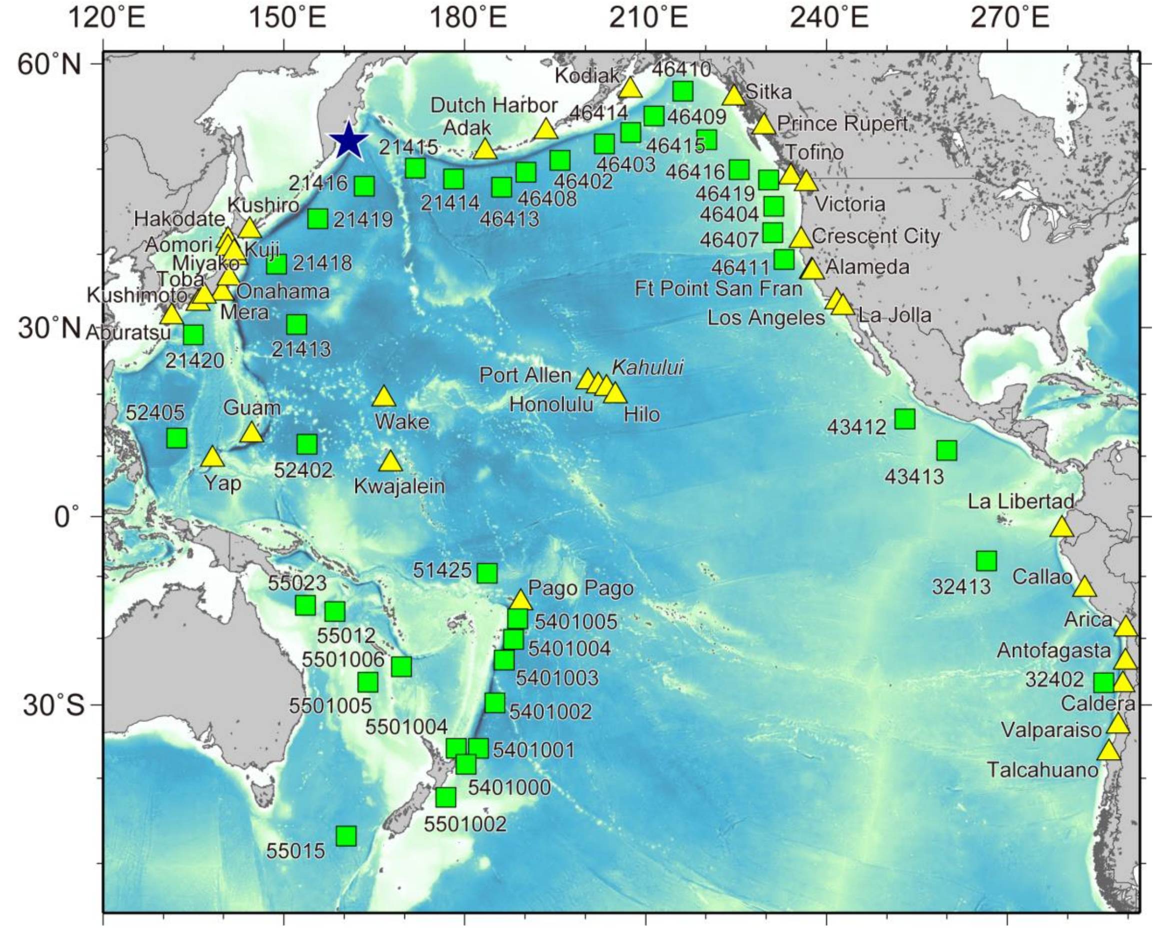

120˚E
150˚E
180˚E
210˚E
240˚E
270˚E
60˚N
30˚N
0˚
30˚S
Kodiak
46410
Sitka
Dutch Harbor
46414
46409
Prince Rupert
Adak
21415
46403
46415
Tofino
46416
21416
21414
46408
46402
46419
Victoria
46413
46404
Kushiro
21419
46407
Crescent City
Hakodate
Aomori
Kuji
21418
46411
Alameda
Miyako
Toba
Onahama
Ft Point San Fran
Kushimoto
Mera
Los Angeles
La Jolla
Aburatsu
21413
21420
Port Allen
Kahului
Honolulu
Hilo
52405
Guam
Wake
43412
52402
Yap
Kwajalein
43413
La Libertad
51425
32413
Callao
55023
Pago Pago
5401005
55012
5401004
Arica
5501006
Antofagasta
5401003
5501005
32402
Caldera
5401002
5501004
Valparaiso
5401001
Talcahuano
5401000
5501002
55015

Figure 1

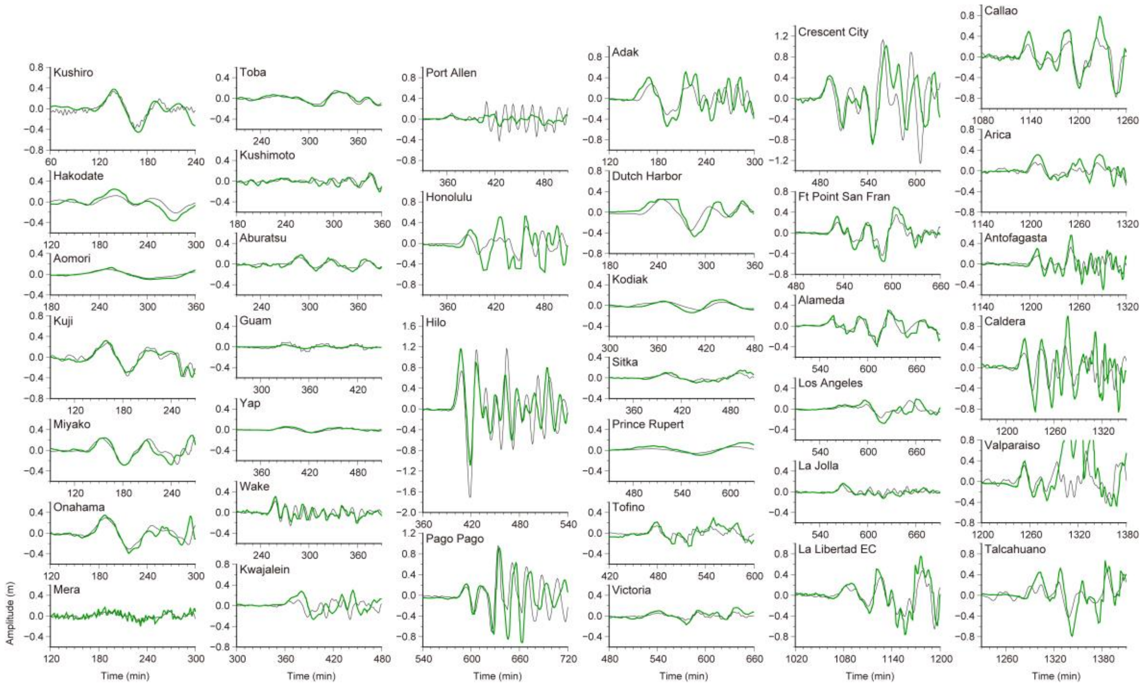
Kushiro
Hakodate
Aomori
Kuji
Miyako
Onahama
Mera
Toba
Kushimoto
Aburatsu
Guam
Yap
Wake
Kwajalein
Port Allen
Honolulu
Hilo
Pago Pago
Adak
Dutch Harbor
Kodiak
Sitka
Prince Rupert
Tofino
Victoria
Crescent City
Ft Point San Fran
Alameda
Los Angeles
La Jolla
La Libertad EC
Callao
Arica
Antofagasta
Caldera
Valparaiso
Talcahuano
Amplitude (m)
Time (min)

Figure 2

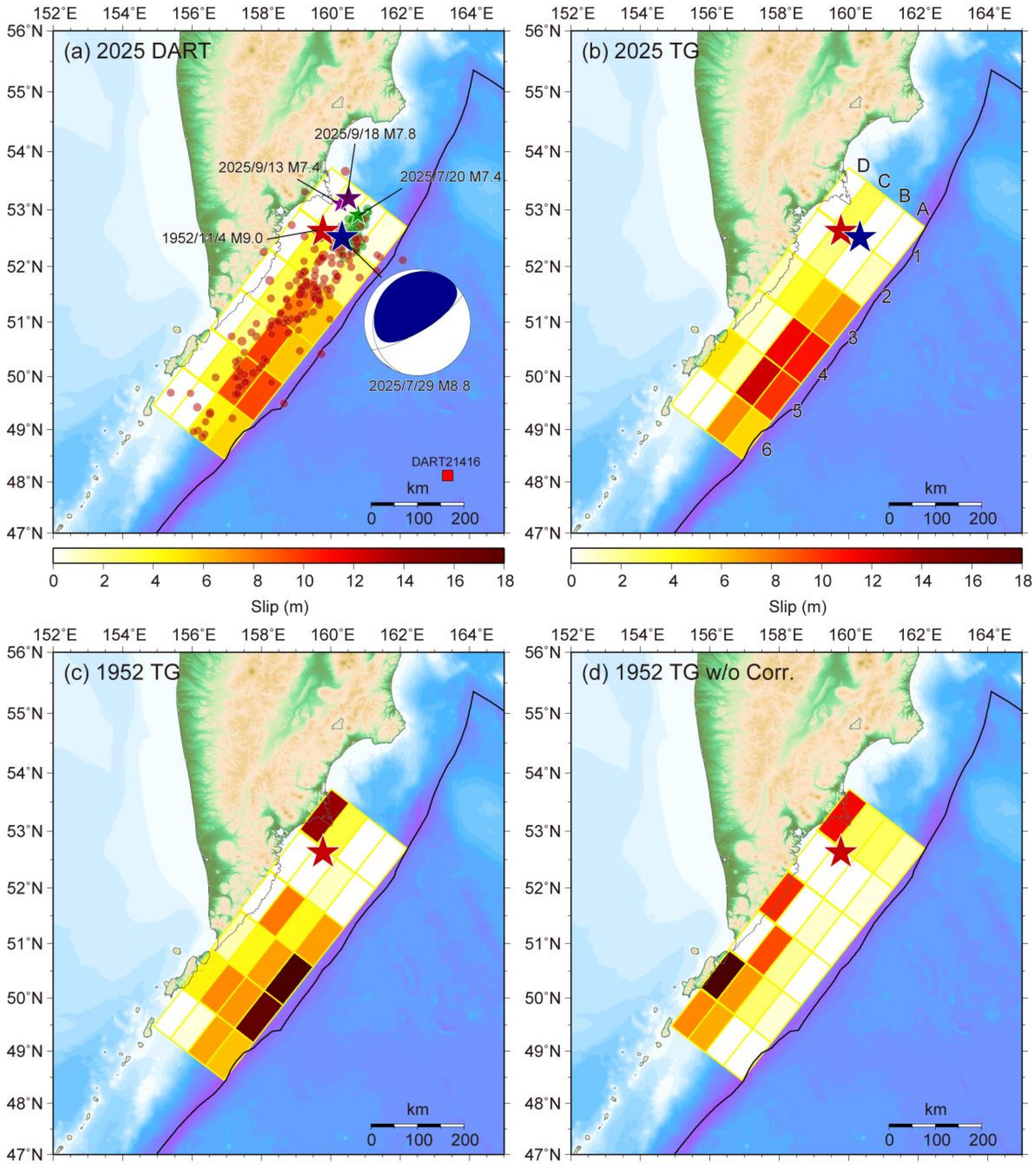
(a) 2025 DART
2025/9/18 M7.8
2025/9/13 M7.4
2025/7/20 M7.4
1952/11/4 M9.0
2025/7/29 M8.8
DART21416
(b) 2025 TG
A
B
C
D
1
2
3
4
5
6
(c) 1952 TG
(d) 1952 TG w/o Corr.
km
0 100 200
Slip (m)
0 2 4 6 8 10 12 14 16 18
152°E 154°E 156°E 158°E 160°E 162°E 164°E
47°N 48°N 49°N 50°N 51°N 52°N 53°N 54°N 55°N 56°N

Figure 3

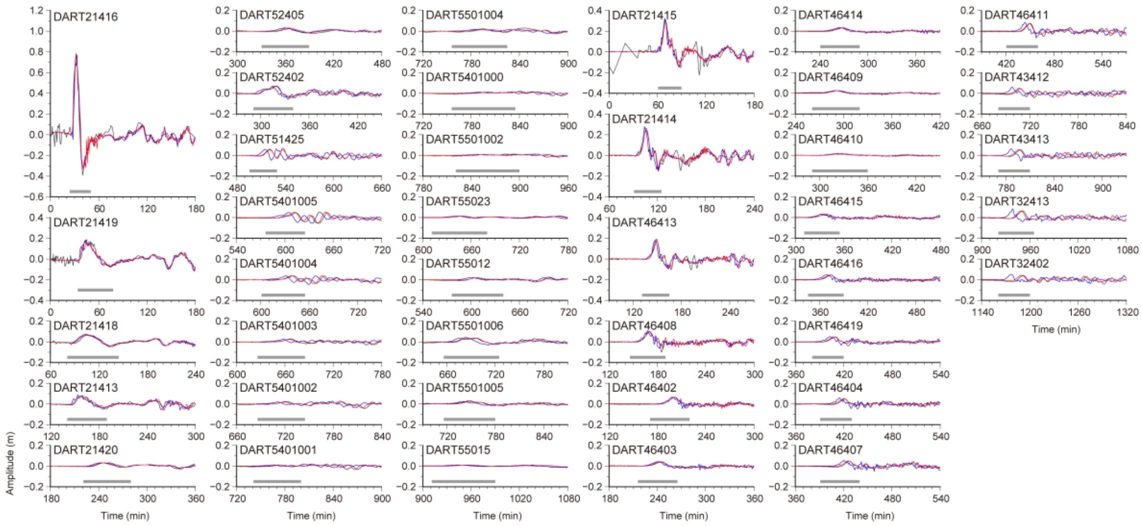
DART21416
DART21419
DART21418
DART21413
DART21420
DART52405
DART52402
DART51425
DART5401005
DART5401004
DART5401003
DART5401002
DART5401001
DART5501004
DART5401000
DART5501002
DART55023
DART55012
DART5501006
DART5501005
DART55015
DART21415
DART21414
DART46413
DART46408
DART46402
DART46403
DART46414
DART46409
DART46410
DART46415
DART46416
DART46419
DART46404
DART46407
DART46411
DART43412
DART43413
DART32413
DART32402
Amplitude (m)
Time (min)

Figure 4

[Geophysical Research Letters]

Supporting Information for

The slip distributions of the 1952 and 2025 Kamchatka earthquakes from tsunami waveforms recorded around the Pacific Ocean

Yushiro Fujii[1] and Kenji Satake[2]

1 International Institute of Seismology and Earthquake Engineering

Building Research Institute, Tsukuba, Japan

2 Department of Earth Sciences, National Central University, Taoyuan, Taiwan

Contents of this file

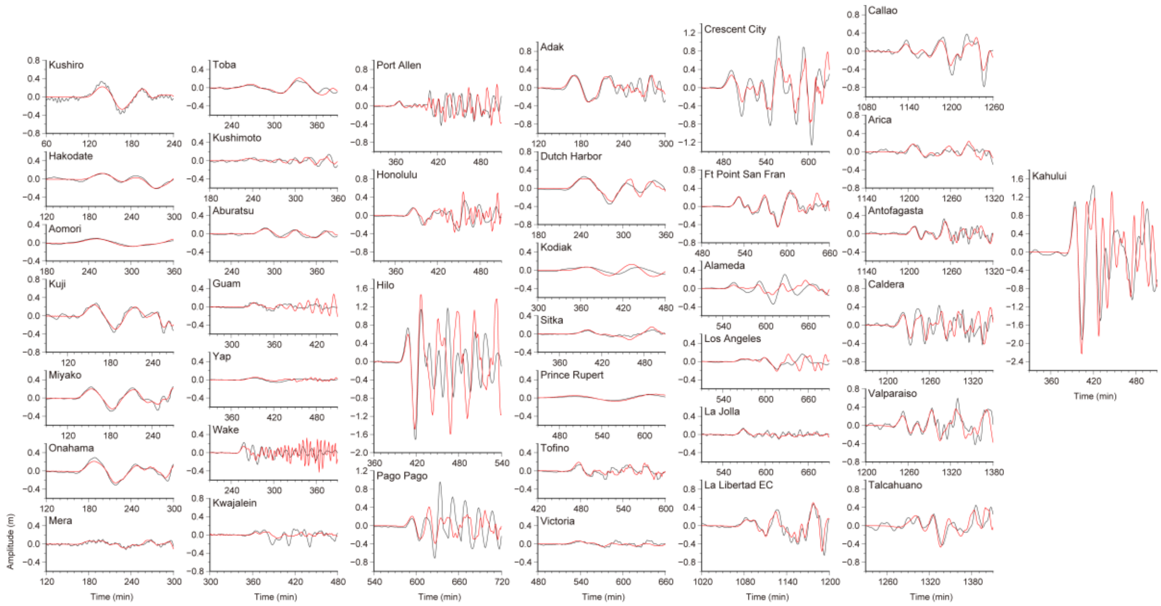

Figure S1: The 2025 tsunami waveforms at tide gauge stations with synthetic waveforms from the DART inversion solution. The black curves are the observations, the red curves are the synthetic waveforms with the corrections for the elasticity of the Earth and sea water.

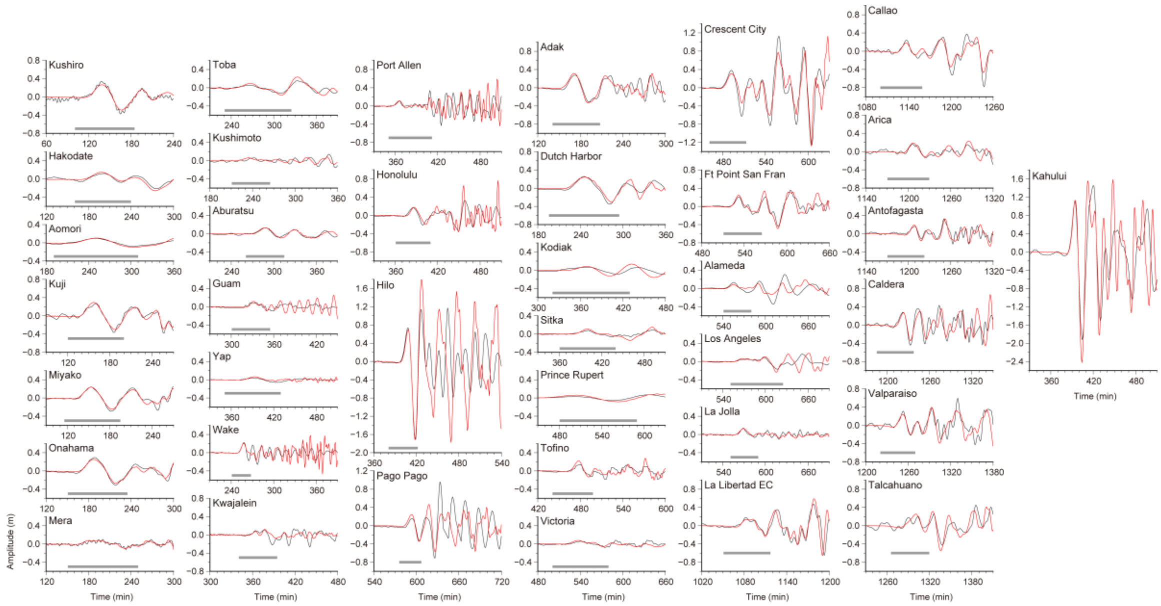

Figure S2: The 2025 tsunami waveforms at tide gauge stations with synthetic waveforms from the TG inversion solution. The black curves are the observations, the red curves are the synthetic waveforms with the corrections for the elasticity of the Earth and sea water. The gray horizontal bars show the time windows used for the inversion.

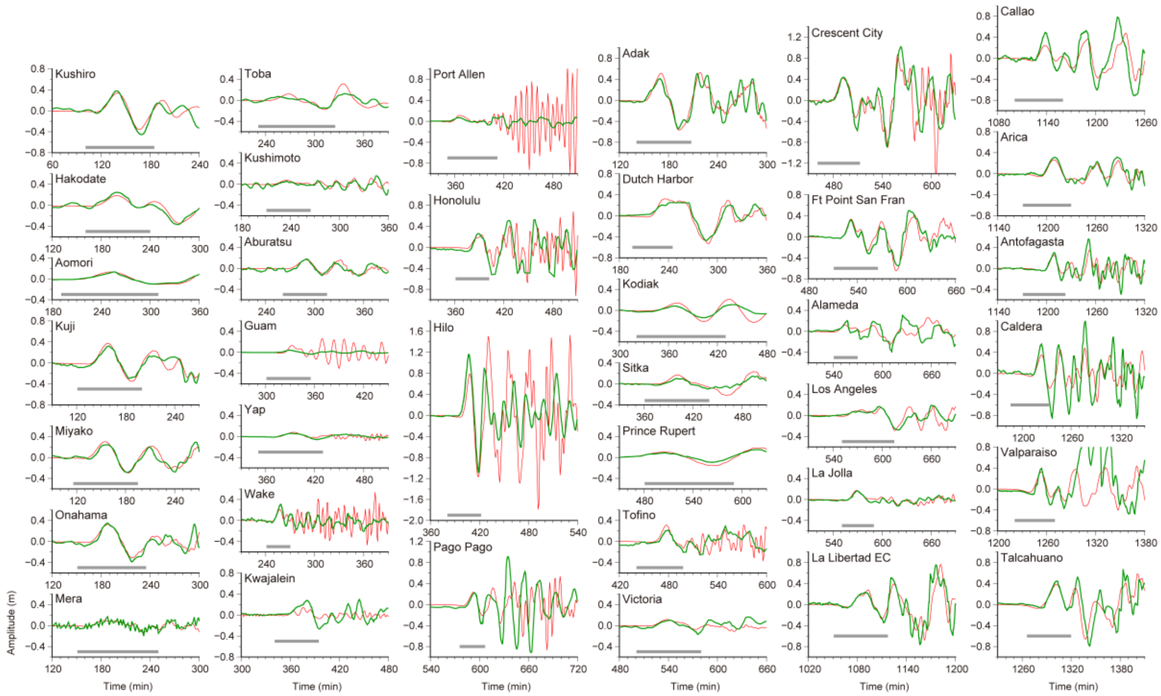

Figure S3: The 1952 tsunami waveforms at the tide gauge stations with synthetic waves from the inversion solution. The green curves are the observations, the red curves are the synthetic waveforms with the corrections for the elasticity of the Earth and sea water. The gray horizontal bars show the time windows used for the inversion.

Table S1 Tide gauges, station corrections, and clock errors for the 1952 earthquake

Name	Data source 2025/1952 Eqs.	Lat. (deg:min)	Lon. (deg:min)	Station corrections (min)	Clock error (min)
Kushiro	IOC/CMO	42:58.4	144:22.0	5	-14
Hakodate	IOC/CMO	41:46.4	140:43.2	3	-2
Aomori	JMA/CMO	40:50.0	140:46.0	10	-9
Kuji	JMA/CMO	40:12.0	141:48.0	3	-31
Miyako	JMA/CMO	39:38.8	141:58.8	4	-18
Onahama	JMA/CMO	36:56.4	140:54.4	4	-10
Mera	IOC/CMO	34:55.2	139:49.2	0	-58
Toba	JMA/CMO	34:29.2	136:49.2	-3	-7
Kushimoto	IOC/CMO	33:28.4	135:46.0	0	1
Aburatsu	IOC/CMO	31:34.8	131:24.8	5	-9
Guam	IOC/USCGS	13:26.4	144:38.8	11	-3
Yap	IOC/USCGS	9:30.4	138:08.0	14	-11
Wake	IOC/NCEI	19:17.6	166:36.8	2	-12
Kwajalein	IOC/NCEI	8:44.0	167:44.0	16	-7
Port Allen	IOC/NCEI	21:53.6	200:24.4	2	4
Honolulu	IOC/USCGS	21:17.6	202:07.6	5	-9
Kahului	IOC/---	20:54.0	203:31.2	4	---
Hilo	IOC/NCEI	19:43.6	204:56.0	5	-10
Pago Pago	IOC/NCEI	-14:16.8	189:18.0	-3	7
Adak	IOC/USCGS	51:51.2	183:22.0	0	-4
Dutch Harbor	IOC/NCEI	53:52.4	193:26.8	3	-15
Kodiak	IOC/USCGS	57:43.2	207:28.0	-5	-7
Sitka	IOC/NCEI	57:02.4	224:39.2	3	-7
Prince Rupert	IOC/NCEI	54:19.2	229:40.8	-20	53
Tofino	IOC/NCEI	49:08.8	234:05.2	5	-5
Victoria Harbor	IOC/NCEI	48:24.8	236:36.0	5	-5
Crescent City	IOC/NCEI	41:44.4	235:48.8	4	-7
Ft Point San Fran	IOC/USCGS	37:48.4	237:32.0	0	-9

Alameda	IOC/USCGS	37:46.0	237:42.0	-1	-1
Los Angeles	IOC/USCGS	33:42.8	241:43.6	5	-4
La Jolla	IOC/USCGS	32:52.0	242:44.4	2	-8
La Libertad EC	IOC/USCGS	-2:13.2	279: 5.2	5	-10
Callao	IOC/USCGS	-12:04.0	282:49.6	6	3
Arica	IOC/NCEI	-18:28.4	289:40.4	6	-9
Antofagasta	IOC/USCGS	-23:39.6	289:35.2	4	-7
Caldera	IOC/USCGS	-27:03.6	289:10.4	5	20
Valparaiso	IOC/USCGS	-33:01.6	288:22.0	3	-6
Talcahuano	IOC/USCGS	-36:42.0	286:53.6	0	-17

Lat. and Lon.: Locations of the tsunami simulation output points on the bathymetry grid data with a grid size of 24 arc-sec

Table S2 Tsunami height from Kamchatka earthquakes

	1737	**1841**	**1952**	**2025**
Kamchatka	5 - 9 m	1 - 15 m	1 - 15 m	0.1 - 18 m
Shumshu Is.	3 m		7 – 23 m	6 – 19 m
Paramushur Is.			5 – 18 m	6 m
Honolulu		1 m	0.6 – 1.5 m	0.3 m
Maui		1 m	1.2 m	1.7 m
Hilo		4.6 m	1.2 - 3.7 m	1.5 m

According to NOAA/NCEI Global Historical Tsunami Data DOI:10.7289/V5PN93H7